Properties of *a*-Si,Ge:H,F alloys prepared by rf glow discharge in an ultrahigh vacuum reactor

J. Kolodzey,[a] S. Aljishi, R. Schwarz, D. Slobodin, and S. Wagner
Department of Electrical Engineering, Princeton University, Princeton, New Jersey 08544

(Received 23 January 1986; accepted 29 June 1986)

a-$Si_{1-x}Ge_x$:H,F alloys with the Ge concentration x ranging from 0 to 1 have been prepared by the rf glow discharge decomposition of SiF_4, GeF_4, and H_2 gas mixtures. An ultrahigh vacuum deposition system has been designed and constructed for the preparation of these alloys. The stainless-steel deposition chamber has Cu gasket-sealed flanges, is turbomolecular pumped, and reaches a base pressure below 10^{-7} Torr (10^{-5} Pa). This deposition system incorporates a load lock which permits short pump-down cycles and which may reduce impurity contamination of the films. The system is described in detail. Compositional, structural, optical, and electronic properties of alloy films made with this system are reported.

I. INTRODUCTION

Hydrogenated amorphous silicon germanium alloys (a-$Si_{1-x}Ge_x$:H) offer great promise for use in photovoltaic devices and for electrophotographic photoconductors.[1,2] Alloying a-Si:H with Ge permits the band gap to be adjusted to the 1.2–1.4 eV range needed by long wavelength absorbers in multijunction solar cells.[3] Photoconductors with a long-wavelength response would allow GaAs LED's or lasers (emitting at 1.43 eV) to be the light sources for image-processing office copiers and for laser printers. Unusual transport properties in amorphous materials may be found in superlattices with controllable band-edge discontinuities.[4,5] Studies of a-Si:H/a-Ge:H superlattices demonstrate that the a-$Si_{1-x}Ge_x$:H alloy system possesses highly perfect heterojunction interfaces.[6]

a-$Si_{1-x}Ge_x$:H alloys have been prepared by glow discharge deposition from SiH_4 and GeH_4,[7] from SiF_4, GeF_4, and H_2,[8] and also by the sputtering of Si and Ge in an H_2 atmosphere.[9] The relative advantages of glow discharge deposition from the hydrides versus the fluorides are not clear, but Shimizu *et al.*[10] have reported encouraging results for the latter: photoconductivity $\sigma_{PH} = 9\times10^{-5}$ S/cm, dark conductivity $\sigma_D = 10^{-8}$ S/cm, normalized photoconductivity $\eta\mu\tau = 10^{-5}$–10^{-6} cm^2/V, and unpaired electron spin density $N_s \leqslant 7\times10^{15}$ cm^{-3} for an $x = 0.3$ alloy. The fluoride source gases have the added advantage of being nonexplosive and of being less toxic than the hydrides.

We are investigating (a-$Si_{1-x}Ge_x$:H,F) alloys to gain a better understanding of their performance as undoped i layers in solar cells. Because of the increasing concern about the effect of impurities on the properties of a-Si:H (Refs. 11 and 12) we have built a system for alloy deposition using ultrahigh vacuum (UHV) techniques.[13] The system incorporates a substrate load lock. Alloy films are deposited by plasma-assisted chemical vapor deposition (CVD) of SiF_4, GeF_4, and H_2 gas mixtures in a radio-frequency (rf) glow discharge. This paper provides a detailed description of this system and presents the properties of a series of alloys.

II. DEPOSITION SYSTEM

We designed and constructed an alloy deposition system with the goal of keeping impurity contamination from air, H_2O, and pump oil vapor to a minimum. This system, shown in Fig. 1, is a flat bed reactor with circular parallel-plate electrodes. The stainless-steel chamber was constructed to UHV specifications.[14] The chamber's inside dimensions are 9 in. in height and $10\frac{3}{4}$ in. in diameter. Copper gasket seals are used on all the flanges. A top view in Fig. 2 shows the flange locations and uses.

The main chamber is pumped by a 170 l/s turbomolecular pump (Balzers TPU 170) which is backed by a rotary mechanical forepump (Alcatel ZM2012AC). The rotary pump has an oil filtration unit (Motor Guard 2X21) with a diatomaceous-earth filter element (Type M-637) for the removal of particles and the neutralization of acid which may collect in the pump oil during deposition. Heating tape wrapped on the chamber walls and on the gas lines desorbs gases and water vapor at 90 °C. The chamber base pressure is less than 10^{-7} Torr (10^{-5} Pa).

Three pressure gauges are used on the main chamber. The turbo inlet pressure is monitored by a wide-range Pirani-type gauge (Convectron 275). The deposition process pressure is monitored by a capacitance manometer (MKS 227). The chamber base pressure is measured with a cold cathode gauge (Varian 860). During deposition the 6-in. outside diameter (o.d.) gate valve between the main chamber and the turbomolecular pump is closed and the process gas flows

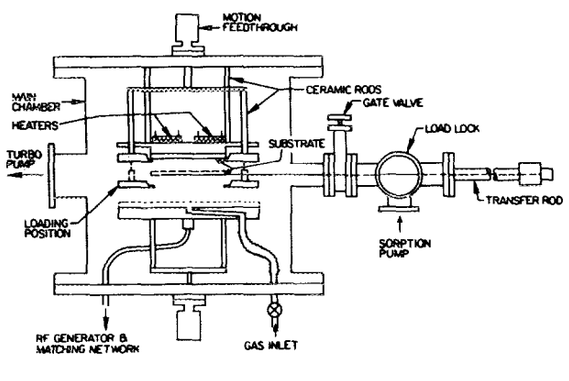

FIG. 1. Layout of the rf glow discharge system used for a-Si,Ge:H,F alloy deposition.

 0734-2101/86/062499-06$01.00

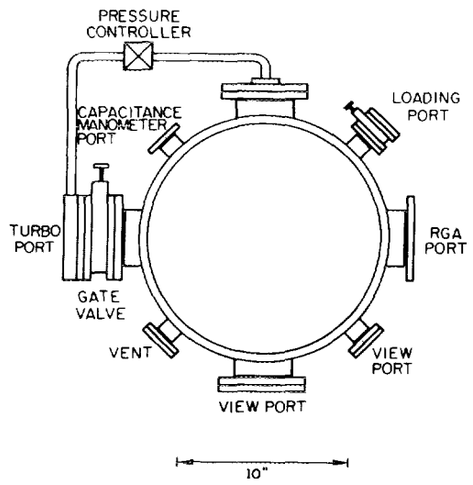

FIG. 2. Top view of the rf glow discharge system showing port usage.

from the chamber through a bypass line, 20 in. long and 1.0-in. diameter, which has a servo-controlled throttle valve (MKS 253A) for process pressure control. A quadrupole mass spectrometer (Inficon Quadrex 100) is used for residual gas analysis. We use it to check the composition of the background gases before deposition and also the purity of the source gases. After the chamber has been opened, exposed to air, and pumped out again, mass 18 (H_2O) shows the largest peak initially. After a deposition run, mass 19 (F) shows the largest peak.

The process gas is supplied to the chamber through the stainless-steel gas manifold which is shown in Fig. 3. Gas from the cylinders is prefiltered (Nupro 4FW) before entering the stainless-steel regulators (Matheson 3600). Stainless-steel tubing ($\frac{1}{4}$ in.) is used throughout and the fittings (Cajon VCR) use Ni metal gaskets. Bellows sealed shut-off valves (Nupro 4BK) are used for isolation. Argon, specified by the supplier (Airco) as grade 99.999% pure, is used for purging the gas regulators, for venting the system to atmospheric pressure, for diluting the process exhaust gases and

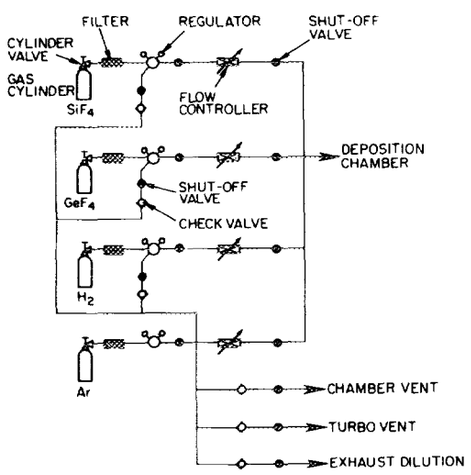

FIG. 3. Gas flow manifold for the rf glow discharge station.

when glow discharge cleaning the chamber. The gas flow rates are set with mass flow controllers (Unit Instruments UFC1000). Inside the chamber the gas line connects to the bottom of the lower electrode by a flexible bellows tubing which has a ceramic break for electrical isolation. The process gas flows from inside the lower electrode out through a series of three stainless-steel diffusing screens (which form the electrode surface plane) to create a uniform flow pattern toward the substrate which is on the upper electrode.

The chamber electrodes are configured as an rf diode, but the electrode wiring is general so that any frequency including dc may be used for excitation. A 1×3 in.^{2} substrate is held upside down on the upper electrode to minimize problems with falling powder or dust. The upper electrode is 11 cm in diameter and is fixed in position relative to the chamber walls. The lower electrode is 10 cm in diameter and can be raised or lowered by a linear motion feedthrough thereby giving an adjustable electrode gap. Both electrodes connect to rf feedthroughs on the chamber via in-vacuum 50-Ω cables so that either electrode can be powered, biased, or grounded. During the experiments reported here, the lower electrode was powered and the upper electrode was either grounded or left floating.

Two ceramic heaters, with printed Fe–Cr resistive patterns (Hittman 528009), are mounted on the top side of the upper electrode for substrate heating. These 1×1 in.^{2} heaters are flat, permit good heat transfer, and have a low outgassing rate under vacuum operation. However, the mechanical connection between the lead wire and printed resistor is weak so that the lead wires come off after about one month of use. Heat transfers from the heaters to the substrate through a Cu thermal distribution block. The substrate temperature, monitored by an iron–Constantan (type J) thermocouple embedded in the Cu block can be controlled up to 400 °C by a relay-type controller (Love 49). This type of controller is used instead of an SCR-type in order to eliminate the reliability problems which stray fields from the rf generator may create with a semiconductor controller.

Springlike retaining tabs (0.01-in. thickness) in the C-shaped movable frame in the upper electrode hold the substrate against the fixed Cu heater block as shown in Fig. 4. When in this deposition-ready position, the substrate is recessed by 0.01 in. (the tab thickness) from the upper electrode surface plane. Three vertical ceramic rods connect this C frame to a bellows sealed linear motion feedthrough which is mounted on the top flange of the chamber. The frame can be raised to hold the substrate in the deposition position or lowered to load or remove a substrate.

The deposition system incorporates a load lock chamber so that samples can be loaded or removed while keeping the main chamber evacuated. An extended chamber bakeout before each run is therefore unnecessary and contamination due to air and water vapor is minimized. A 2.75-in.-o.d. gate valve connects the load lock to the main chamber. The load lock is pumped independently of the main chamber by a liquid-nitrogen-cooled sorption pump (Varian Vacsorb). A ceramic heater in the load lock can be used to bake out the substrate and the load lock chamber prior to loading.

For loading, a substrate is placed onto a pallet in the load lock through the elastomer sealed front port which has an o.d. of 5.12 in. This pallet is mounted on the end of a magnetically coupled UHV transfer rod (Riber TLTM64-500) as shown in Fig. 4 and holds the 1×3 in.^{2} substrate for transfer to the chamber or for sample removal. After the load lock has been pumped down to below 10 mTorr the gate valve to the main chamber is opened. The transfer rod moves the sample to a specific position between the fixed upper electrode heater block and the movable upper electrode C frame which has been previously lowered to the loading position. Figure 5 shows a substrate on the transfer rod pallet with the frame in this lower position. As the frame is raised it passes the transfer rod pallet, and the spring tabs lift off the substrate. As the frame is raised farther, the tabs pull the substrate firmly against the Cu heater block. Although this is a routine operation, it is advisable to observe the pallet and the electrode frame through the front viewport (Fig. 2) for precise positioning. This 6-in.-o.d. viewport is provided with a Venetian blind shutter to prevent *a*-Si deposition on its window. The electrodes and the substrate are now in the deposition position. The movable frame has sufficient clearance to accommodate a wide range of substrate thicknesses, but 1 mm is typical. With substrate loading thus completed the transfer rod pallet is then withdrawn into the load lock, the load lock gate valve is closed and deposition can begin.

For sample removal after deposition the transfer rod pallet is again placed under the upper electrode but this time with the frame still in the raised (deposition) position. The frame is lowered placing the sample onto the pallet and is lowered farther to the position shown in Fig. 5 so as to be clear of the pallet which can then be withdrawn into the load lock for sample removal.

III. ALLOY PREPARATION

We have found that an extremely clean substrate is required to eliminate peeling and to prevent the formation of pinholes in the films. A 1×3 in.^{2} glass substrate (Corning 7059) is first ultrasonically cleaned in a hot detergent-deionized (DI) H_2O solution followed by a DI-H_2O rinse. It is vapor degreased with isopropyl alcohol and a 10- or 50-nm Cr coating is then thermally evaporated (Edwards 306A vacuum coater) onto a 1×1.5 in.^{2} masked-off area on the glass surface for use as a back contact during electrical measurements. After evaporation the substrate is rinsed in a sequence of 1,1,1 trichloroethane, acetone, is vapor degreased, and immediately placed into the load lock which is then evacuated. After loading into the main chamber the substrate is baked at 270 °C for about 1 h until the chamber pressure is less than 10^{-7} Torr. The substrate is next glow discharge cleaned in Ar for 5 min, and is ready for deposition.

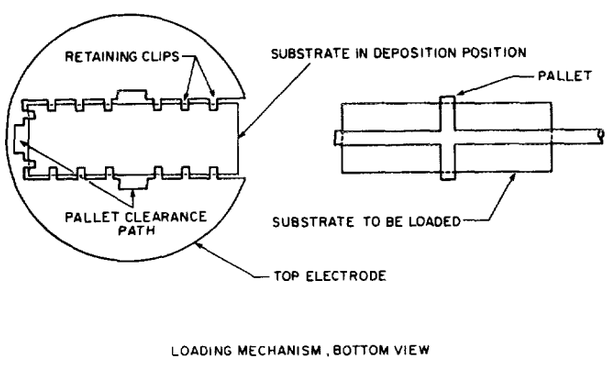

FIG. 4. Detail of the loading mechanism for the rf glow discharge station.

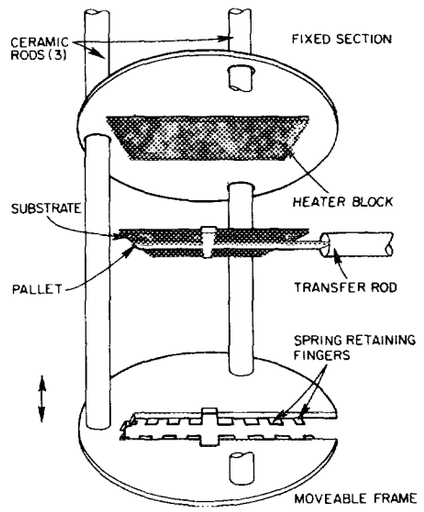

FIG. 5. Detail of the upper electrode with frame and substrate pallet in loading position.

For *a*-$Si_{1-x}Ge_x$:H,F alloy preparation a SiF_4, GeF_4, and H_2 gas mixture is decomposed in an rf glow discharge at 13.56 MHz. Highest purity source gases are used. The SiF_4 is specified by the supplier (Matheson) as 99.99% pure and the H_2 is specified as 99.9999% (Airco). The GeF_4 is only grade 99% (Ozark-Mahoning, batch estimate); the principal impurities from mass spectroscopy analysis are SiF_4 and H_2O. For the experiments reported here the SiF_4 flow during deposition is maintained at 21 standard cubic centimeters per minute (sccm) and the H_2 flow is set to a value between 3 and 12 sccm. The alloy composition is controlled by the GeF_2 flow which is set in the range from 0–0.6 sccm. Deposition process pressure is typically 0.11 Torr. Higher deposition pressures cause film peeling.

The glow discharge is powered by a 300-W rf power generator (ENI HF300). The generator output power is reduced to deposition levels[15] by a 10-dB attenuator (Bird 8343). A ham radio antenna tuner (Heathkit SA 2060A) matches the 50-Ω rf generator output impedance to the load impedance constituted by the discharge electrodes. The voltage standing-wave ratio can routinely be tuned to a value less than 1.1 and the reflected power is less than 0.1 W. The forward and reflected power is measured by an in-line wattmeter (Bird 43). Deposition power is set in the range from 5 to 25 W total giving a power density at the substrate of 50 to 250 mW/cm^2. The gap between the upper (substrate) electrode and the lower (gas-diffusing screen) electrode was set at 3.7 cm. Smaller gaps cause a nonuniform circular (bull's eye) deposition pattern on the substrate which was found to be inde-

pendent of the gas flow direction. Process temperature was set at 270 °C measured by the thermocouple in the Cu heater block. The temperature at the substrate surface itself is uncalibrated, and may be 30–40 °C lower.

The deposition duration is timed to give a desired film thickness with a typical run lasting several hours for a 1-μm film. The deposition rate increased with the GeF_4 gas mixture ratio as shown in Fig. 6 with the other deposition conditions being 5-W power, 0.11-Torr pressure, 270 °C temperature and the flow rate and other parameters as given above.

After deposition the sample cools for about 1 h in the chamber. This is achieved without shutting off the substrate heaters by lowering the electrode frame about 2 cm away from the heater block (maintaining the heaters at a constant temperature prolongs their life). The sample is then removed from the chamber and cools another hour in the load lock.

IV. ALLOY PROPERTIES

Our goal is to understand the alloy deposition parameters which yield device grade material. We evaluated the compositional, structural, optical, and electronic properties of the alloy films. The film composition was determined by Auger electron spectroscopy along with argon ion beam sputter profiling to check for differences between surface and bulk composition. A thin oxide layer of thickness 2–8 nm was typically found on the surface. An *a*-Si, Ge:H alloy reference standard was used to calibrate the Auger peak heights. The composition of this standard had been determined by elastic scattering of 12-MeV protons (nuclear elastic scattering or NES).[16] Film composition versus the normalized GeF_4 flow rate is shown in Fig. 7. One pure Si film ($x = 0$) which was analyzed by NES has an H concentration of 2.36% and an F concentration of 2.89%. The composition of the films was also checked by secondary ion mass spectroscopy (SIMS). The films were found to contain O, C, and F but the exact quantities could not be calibrated due to matrix effects which result in a different number of counts per a given constituent concentration depending on the different Si/Ge ratio of the alloys. The film composition was found to be uniform with depth.

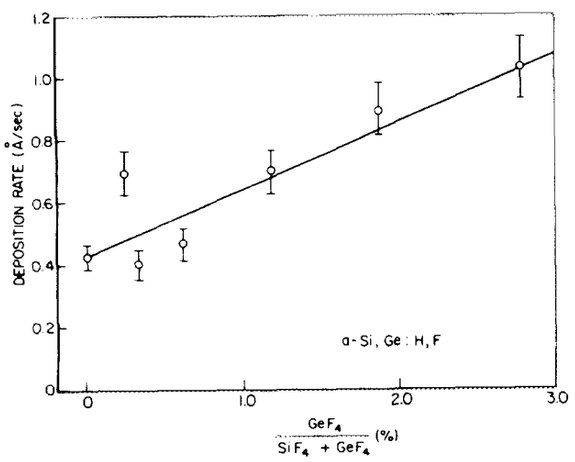

FIG. 6. Film growth rate as a function of the normalized GeF_4 flow rate.

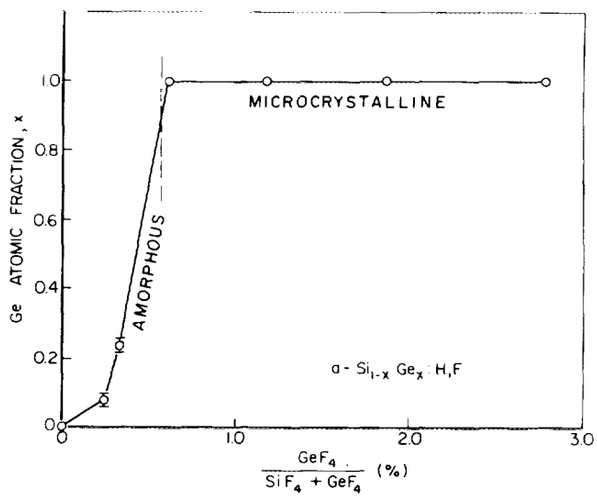

FIG. 7. Ge concentration as a function of the normalized GeF_4 flow rate.

The alloy film structure was analyzed by Raman scattering with an Ar ion laser probe exciting at 514.5 nm, and by x-ray diffraction using the Cu $K\alpha$ line at 1.54 Å. The penetration depth of the Raman probe light is about 0.1 μm. Except for the pure Ge films, most samples were at first thought to be amorphous as evidenced by the absence of an optical phonon peak in a plot of the Raman intensity versus wave number ($\bar{\lambda}$). X-ray diffraction, however, revealed that some of the films which appeared to be amorphous by Raman scattering in fact showed small-intensity peaks at the crystalline (*c*) diffraction angles. For *c*-Si these angles are $2\theta = 28.5°$ (111 plane), 47.3° (220 plane), and 56.2° (311 plane); for *c*-Ge: $2\theta = 27.4°$ (111), 45.5°(220), and 53.9°(311). For samples deposited onto Cr, x-ray peaks due to the Cr may also appear at $2\theta = 44.7°$. Some alloys possessed a microcrystalline structure with a grain size estimated by Scherrer's formula to be in the range of 8 to 36 nm. This structure versus composition is noted in Fig. 7. The pure Ge films tended to be microcrystalline (μc). One pure Ge film is amorphous at the top surface and microcrystalline near the glass substrate. The Raman spectrum for this film at the top surface showed a spectrum characteristic of amorphous Ge; the bottom spectrum taken through the glass substrate showed a microcrystalline peak at $\bar{\lambda} = 298\ cm^{-1}$.

The optical absorption coefficient α is determined from reflection and transmission spectra which are measured with light from a quarter-meter double grating monochromator (Jarrel–Ash Monospec 27) using a 150-W tungsten–iodine lamp source (Oriel). This light is chopped (Ithaco HMS 220) at 45 Hz and detected with a lock-in amplifier (EG&G 5602) using both Si and Ge photodetectors to cover the entire spectral range of interest (600–1600 nm). The monochromator and the lock-in have IEEE-488 bus interfaces and an HP-87 computer performs automatic absorption data acquisition. The film thickness was determined from the transmission interference fringe spacing at infrared wavelengths

and was checked with a step profilometer (Tencor Alphastep).[17] We have found it necessary to measure thickness in the infrared where the interference minima and maxima have constant value rather than at visible wavelengths. Measurement in the visible gives an apparent thickness value which is about 20% larger than the true value due to an underestimate of the fringe spacing because of the steep increase of transmission with wavelength at the absorption edge, and also due to the change of refractive index with wavelength. The optical gap E_{opt} was determined by the intercept of $\sqrt{\alpha h\nu}$ versus photon energy $h\nu$ (Tauc's method) as shown in Fig. 8. The three amorphous samples show straight lines giving E_{opt} as the energy axis intercept. The four μc-Ge samples show irregular curves because the Tauc relation between α and $h\nu$ does not apply to microcrystalline material. Instead, the energy axis intercepts for the μc-Ge samples will be taken as empircal numbers for bookkeeping purposes for use in other plots in this paper. All the E_{opt} values are plotted versus the normalized GeF_4 flow rate in Fig. 9. E_{opt} decreases with increasing GeF_4 flow from 1.75 eV for a pure Si film to about 0.9 eV for the pure Ge films. At low GeF_4 flow rates the drop in E_{opt} with Ge content is steep for the amorphous films. At the higher GeF_4 flow rates (μc films) this slope is significantly less steep.

Dark conductivity σ_D and incremental photoconductivity $\Delta\sigma_{PH}$ are measured using coplanar geometry contacts 1.1 cm long with a 0.16-cm gap. These contacts are 100-nm-thick evaporated Al or Cr stripes. A voltage ranging from 10–200 V is applied (Kepco 188) which gives a current reading in excess of 0.1 nA. The current is measured with either an electrometer (Keithley 619) or a picoammeter (Keithley 417). The contacts exhibit ohmic behavior as deduced from the linear current–voltage characteristics. The conductivities are plotted as a function of E_{opt} in Fig. 10. The dark conductivity increases abruptly from 10^{-9} to 10^{-2} S/cm at $E_{opt} \sim 1.5$ eV as the Ge contact x increases. This abrubt increase in conductivity is associated with the transition in the films from an amorphous to a microcrystalline structure and is not due simply to the increased Ge content. We are currently investigating the conductivity of Ge-rich films versus structure.

Photoconductivity is measured by illuminating the films with monochromatic light with the light intensity and wavelength selected to give a constant photon absorption rate of 2×10^{21} photon $cm^{-3}\,s^{-1}$. Interference filters with wavelength passbands centered at 600, 650, and 750 nm are selected depending on E_{opt} to ensure uniform absorption within the film. The photoconductivity is in the 10^{-3} to 10^{-5} S/cm range as shown in Fig. 10, varying only slightly with E_{opt}.

The diffusion length is an important indicator of how the material will perform in a device structure such as a photovoltaic cell. The ambipolar diffusion length L_D, plotted as a function of E_{opt} in Fig. 11, decreases with increasing Ge content x. The values range from 0.1 to 0.45 μm. The two *a*-Ge:H films have a very low photovoltage and were measured without bias light; their L_D is close to zero. The L_D value for a film made from SiH_4 rather than the fluorides is also shown for comparison. The diffusion length is measured by the differential surface photovoltage (SPV) method.[18] The surface Schottky barrier is formed with semitransparent 10–20 nm

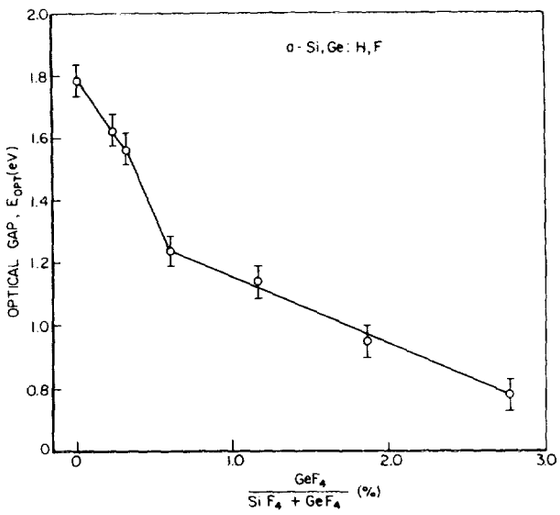

FIG. 9. Optical energy gaps of the alloys vs the normalized GeF_4 flow rate.

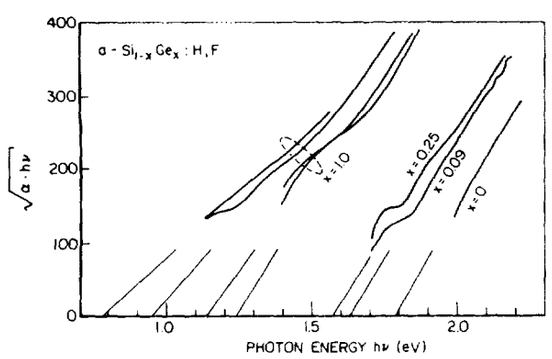

FIG. 8. Optical absorption spectra plotted in the Tauc form vs photon energy.

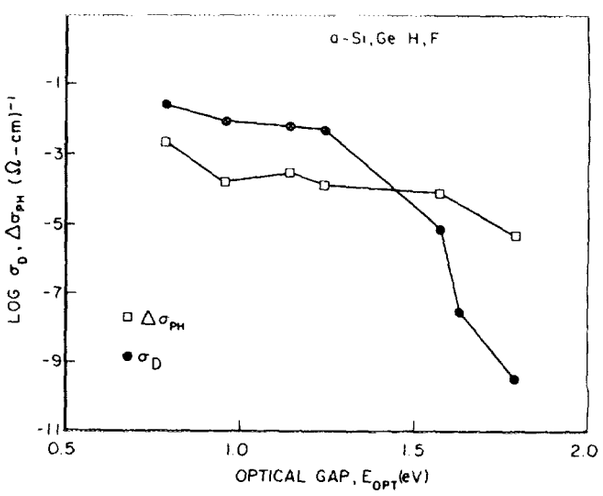

FIG. 10. Dark conductivity σ_D and photoconductivity increment $\Delta\sigma_{PH}$ for the alloys as functions of E_{opt}.

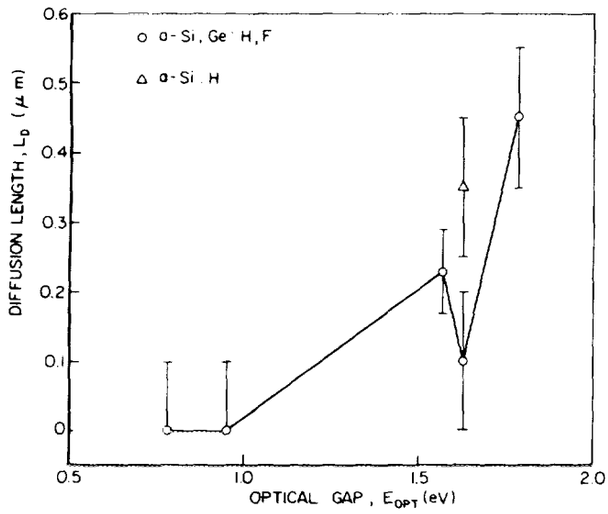

FIG. 11. Minority carrier diffusion length of the alloys as a function of E_{opt}.

Pd dots which are thermally evaporated onto the film surface. The back contact is the 10–50 nm Cr coating on the glass substrate. A bias light of 30–100 mW cm^{-2} or more is used to ensure collapse of the surface space charge layer width. Only then is the drift contribution to the surface photovoltage reduced so that the measured apparent L_D is the true value. The required bias intensity is determined by plotting the apparent diffusion length against the (linear) bias intensity and using intensity values for which the slope of L_D decreases to give a flat curve. Otherwise a comparison of values for different samples can be made only if the same bias intensity has been used for the measurements. Care must be taken that the bias light intensity is not too high because of errors which may be introduced due to the intensity dependence of L_D.[19] The ambipolar, rather than the minority carrier, diffusion length appears in the diffusion equation for near intrinsic semiconductors and for conditions of high-level injection when the electron and hole concentrations are approximately equal. For *a*-Si:H in which it is expected that the electron mobility is much greater than the hole mobility and the ratio of free to trapped electrons is much greater than the ratio of free to trapped holes, the ambipolar diffusion length is given by[20]

$$L_D = \sqrt{\frac{2kT}{q}\mu_p \tau_p} = \sqrt{2} L_p, \tag{1}$$

where k is Boltzmann's constant, T is the temperature, q is the electronic charge, μ_p is the minority carrier (hole) mobility, τ_p is the hole lifetime, and L_p is the hole diffusion length. Therefore the measured L_D is approximately equal to the hole diffusion length.

V. SUMMARY

An ultrahigh vacuum system for the rf glow discharge deposition of *a*-$Si_{1-x}Ge_x$:H,F alloys has been designed and constructed. A load lock attached to the main chamber permits samples to be loaded and removed under vacuum. Therefore the pump-down time is reduced and contamination from air is minimized.

Alloy preparation by the decomposition of SiF_4, GeF_4, H_2 source gases results in good electronic properties for samples with $E_{opt} > 1.5$ eV. An initial series of films with lower optical gaps and increased Ge content has a μc structure and poor electrical properties. Photoconductivity varies little with E_{opt}. Dark conductivity rises abruptly with decreasing E_{opt} at 1.5 eV for the μc-Ge samples. The ambipolar diffusion length is several tenths of a μm for the pure Si samples and decreases with increasing Ge content. The transport behavior of these alloys with changing Ge concentration is being investigated.

ACKNOWLEDGMENTS

We appreciate and acknowledge B. Abeles, R. D'Aiello, H. Deckman, R. Dickson, T. Moustakas, H. Stasiewski, and C. Wronski for helpful discussions; A. Kahn, K. Stiles, and D.-W. Tu for help with Auger spectroscopy; P. Fauchet, I. Campbell, and C.-H. Yang for Raman measurements; C. Magee for secondary ion mass spectroscopy; C. Crider and S. Schafer for advice on vacuum technology; and V. Chu, S. Quinlan, and D.-S. Shen for help with sample preparation and characterization. The research on alloys of *a*-Si:H at Princeton University is supported by the Electric Power Research Institute.

[a] Eastman Kodak Graduate Fellow. Present address: Department of Electrical Engineering, University of Illinois, Urbana, IL 61801.

[1] *Amorphous Semiconductor Technologies and Devices* [Jpn. Annu. Rev. Electron. Comput. Telecommun. **2** (1982), **6** (1983), **16** (1984)].
[2] *Hydrogenated Amorphous Silicon*, Semiconductors and Semimetals, Vol. 21, Pts. A–D, edited by J. I. Pankove (Academic, New York, 1984).
[3] E. A. DeMeo and R. W. Taylor, Science **224**, 245 (1984).
[4] T. Tiedje, B. Abeles, and B. G. Brooks, Phys. Rev. Lett. **54**, 2545 (1985).
[5] S. Wagner, Jpn. J. Appl. Phys. **24**, L155 (1985).
[6] B. Abeles, T. Tiedje, K. S. Liang, H. W. Deckman, H. C. Stasiewski, J. C. Scanlon, and P. M. Eisenberger, J. Non-Cryst. Solids **66**, 351 (1984).
[7] K. D. Mackenzie, J. R. Eggert, D. J. Leopold, Y. M. Li, S. Lin, and W. Paul, Phys. Rev. B **31**, 2198 (1985).
[8] K. Nozawa, Y. Yamaguchi, J. Hanna, and I. Shimizu, J. Non-Cryst. Solids **59&60**, 533 (1983).
[9] R. A. Rudder, J. W. Cook, Jr., and G. Lucovsky, Appl. Phys. Lett. **45**, 887 (1984).
[10] S. Oda, Y. Yamaguchi, J. Hanna, S. Ishihara, R. Fujiwara, S. Kawate, and I. Shimizu, in *Proceedings of the Vacuum Science and Engineering Conference; Kobe, Japan, 1984* [Tech. Dig. Int. **B-IIp-8**, 429 (1984)].
[11] C. C. Tsai, J. C. Knights, R. A. Lujan, B. Wacker, B. L. Stafford, and M. J. Thompson, J. Non-Cryst. Solids **59&60**, 731 (1983).
[12] Y. Kuwano, M. Ohnishi, S. Tsuda, Y. Nakashima, and N. Nakamura, Jpn. J. Appl. Phys. **24**, 413 (1982).
[13] J. Kolodzey, S. Aljishi, R. Schwarz, and S. Wagner, Electrochemical Society Spring Meeting, Toronto, 12–17 May 1985, Abstract No. 176.
[14] Dr. C. Crider, Princeton Research Instruments Inc., P. O. Box 1174, Princeton, NJ 08540.
[15] Recommended by Dr. B. Abeles of Exxon Research.
[16] R. Schwarz, S. Wagner, R. T. Kouzes, and R. D. Wieting, Appl. Phys. Lett. **46**, 552 (1985).
[17] Courtesy of Dr. C.-L. Shieh at Siemens Research Laboratory, Princeton, NJ.
[18] R. Schwarz, D. Slobodin, and S. Wagner, Appl. Phys. Lett. **47**, 740 (1985).
[19] M. Hack and M. Shur, J. Appl. Phys. **55**, 2967 (1984).
[20] A. Moore, in Ref. 2, Vol. C, Chap. 7, pp. 239–256.